Printed in U.S.A.

73-HT-43

an ASME publication

$3.00 PER COPY

$1.00 TO ASME MEMBERS

Apparent Conductivity of Glass Microspheres from Atmospheric Pressure Vacuum

M. M. YOVANOVICH

Professor of Mechanical Engineering,
Thermal Engineering Group,
University of Waterloo,
Waterloo, Ontario,
Canada
Mem. ASME

An analytical study is presented for predicting the apparent thermal conductivity of beds of uniform diameter glass microspheres. The mathematical model is based upon thermal constriction resistance within the spheres and conduction resistance of an effective gas gap thickness. Both decoupled and coupled models are considered, and the latter is shown to be superior to the former. The theory is valid for gas pressures ranging from vacuum conditions to atmospheric. There is good to excellent agreement between the coupled model and available experimental data.

Contributed by the Heat Transfer Division of The American Society of Mechanical Engineers for presentation at the ASME-AIChE Heat Transfer Conference, Atlanta, Ga., August 5-8, 1973. Manuscript received at ASME Headquarters April 23, 1973.

Copies will be available until June 1, 1974.

Apparent Conductivity of Glass Microspheres from Atmospheric Pressure Vacuum

M. M. YOVANOVICH

ABSTRACT

An analytical study is presented for predicting the apparent thermal conductivity of beds of uniform diameter glass microspheres. The mathematical model is based upon thermal constriction resistance within the spheres and conduction resistance of an effective gas gap thickness. Both decoupled and coupled models are considered, and the latter is shown to be superior to the former. The theory is valid for gas pressures ranging from vacuum conditions to atmospheric. There is good to excellent agreement between the coupled model and available experimental data.

NOMENCLATURE

a radius of circular contact, m

a^* dimensionless contact radius (2a/D)

D diameter of spheres, m

E modulus of elasticity of spheres, N/m^2

F contact force, N

k_a apparent thermal conductivity of microspheres, W/m K

k_g apparent thermal conductivity of gas (air), W/m K

$k_{g\infty}$ apparent thermal conductivity of gas at atmospheric pressure, W/m K

k_s bulk thermal conductivity of glass spheres, W/m K

k_a^* dimensionless apparent conductivity (k_a/k_s)

k_{av}^* dimensionless apparent conductivity at vacuum conditions

k_g^* dimensionless fluid conductivity (k_g/k_s)

L dimensionless parameter (D/2a)

P_g gas pressure, mm Hg

P_g^* reduced gas pressure (Pg/760)

Q heat flow rate, W

Q_c heat flow rate via the contact area, W

Q_g heat flow rate via the gas, W

R thermal resistance, K/W

R_c thermal constriction resistance, K/W

R_g gas resistance, K/W

R_r radiation resistance, K/W

T temperature, K

T_c contact area temperature, K

T^* reduced absolute gas temperature (T/288)

x dimensionless radial position (r/a)

Λ mean free path of air at atmospheric pressure, m

Λ^* dimensionless mean free path (Λ/D)

α accommodation coefficient parameter, $\left[\frac{\alpha - \alpha_1}{\alpha_1} - \frac{2 - \alpha_2}{\alpha_2}\right]$

δ equivalent air gap thickness, m

δ^* dimensionless air gap thickness (δ/D)

δ_e^* equivalent dimensionless air gap thickness (δ_e/D)

δ_{e1}^* equivalent dimensionless air gap thickness for close packed spheres

δ_{e2}^* equivalent dimensionless air gap thickness for loose packed spheres

ψ thermal constriction factor

ν Poisson's ratio

ξ lower limit of integration

ϕ porosity of the system

Φ_1 dimensionless parameter defined by Eq. (8)

Φ_2 dimensionless parameter defined by Eq. (18)

INTRODUCTION

Since the turn of this century scientists and engineers have been interested in heat transfer through porous substances [1]. In general these porous substances have consisted of solid particles of various shapes and sizes in physical contact with each other, and voids of even more complicated shape. The two methods of predicting the apparent conductivity of these complex heterogeneous substances are 1) the method of generalized thermal conductivities and 2) the method based upon the geometry of a typical element. In the method of generalized conductivities it is postulated that the effective thermal conductivity depends upon a) the thermal conductivities of the solid and fluid in the voids, b) the volume concentrations of the solid and fluid, and c) the distribution of the two phases within the porous substance. In the second method one assumes a typical particle shape and size, a typical packing and calculates the heat transfer through such an element. The first method has been used with some success to predict the effective or apparent thermal conductivity of very porous substances consisting of complex shaped solid particles and a fluid whose thermal conductivity is not greatly different from the solid. It cannot be used to predict the conductivity of closely packed substances when the thermal conductivities of the solid and fluid are quite different. The second method has been employed in recent studies to predict with considerable success the apparent conductivity of porous substances whose particles have well-defined geometries.

This study will be based upon the second method and will consider the effect of air pressure upon the apparent conductivity of glass microspheres. The analysis will be based upon the simplest cubic packing, and will consider uncoupled and coupled heat flows through the solid and gas phases.

Related Studies

Heat transfer through composite materials such as powders, sand, rocks, ceramics, shot and more recently glass beads has been under experimental and analytical investigation during the past two decades [2-11, 15]. Argo and Smith [2] conducted an experimental and analytical study to determine the effect of gas flow rates upon the apparent conductivity of spherical and cylindrical beds. Yagi and Kunii [3] studied the effect of a motionless fluid upon the apparent conductivity of beds with various kinds of packing: iron spheres, porcelain packings, cement clinker, insulating brick, and Raschig rings. Kunii and Smith [4] derived equations for predicting the apparent conductivity of beds of unconsolidated particles containing stagnant fluid. They modelled the particles as identical sized spheres making point contact; i.e., they assumed that all the heat was transferred between adjacent spheres by means of the fluid and radiation across the fluid gap. Their theory appeared to agree well only with test data obtained with solids and saturating fluids having similar conductivities, but the theory fails to predict the apparent conductivity at gas pressures below one atmosphere and under vacuum conditions. Woodside and Messmer [5] conducted a rather extensive experimental study to ascertain the apparent conductivity of several unconsolidated samples: three quartz sand packings, a glass bead packing, and a lead shot packing. They also investigated the effect of saturating fluid conductivity as well as the pressure of the saturating gas. They used the theoretical results of Yagi and Kunii [3], and Kunii and Smith [4] with some modifications to predict the apparent conductivity of unconsolidated packings when the gas pressure is one atmosphere. They made no attempt to correlate the apparent conductivity at low gas pressures for consolidated packings. Chen and Churchill [6] examined the effect of high temperature (>800 F) radiation heat transfer through beds of glass, aluminum oxide, steel and silicon carbide spheres, cylinders and irregular grains. They concluded that radiation effects are only important for temperatures above 1600 F. Dumez [7, 8] determined the apparent conductivity of glass microspheres over a wide range of temperatures and gas pressures. He showed that radiation heat transfer is negligible for sphere diameters of 400 μ even when the temperature of the spheres approaches 400 C. Dumez attempted to correlate the test data against the theoretical results of Kunii and Smith [4]. He found reasonable agreement only at atmospheric pressure. He was unable to correlate the data for low gas pressures, especially at vacuum conditions, because Kunii and Smith based their theory on point contact between spheres. Luikov et al [9] examined, both empirically and analytically, the apparent thermal conductivity of powdered and solid porous materials over a wide range of temperatures, pressures, and types of saturating fluids. They compared their test results with theories proposed by other investigators as well as their own theory which included the effect of contacts. This theory is much too complicated because it attempts to include the effect of surface roughness, the effect of oxides, various packing models as well as the effect of gas pressure. They made no attempt to correlate their test data and their theory over the entire range of gas pressure. They showed excellent agreement with some substances, moderate agreement with others, and some very poor agreement (errors > 170%) with steel balls in hydrogen. Wakao et al [10] determined the view factor between contacting hemispheres which can be used to predict the effect of radiation heat transfer when it is important. Masamune and Smith [11] obtained apparent conductivities of beds of spherical glass beads having uniform diameters ranging from 29 to 470 microns. Data were obtained at numerous air pressure levels ranging from 10^{-2} to 760 mm Hg. All tests were conducted at an average bed temperature of 315 K. Their analysis was essentially an extension of the Kunii and Smith model [4] with an attempt to include empirically the effect of contacts.

ANALYSIS

The analyses, both decoupled and coupled, will be based upon the geometry of Fig. 1 which shows two spherical particles in elastic contact with each other. It is assumed that the particles are surrounded by a motionless fluid. Heat transfer can occur between the isothermal planes T_1 and T_2 by the following mechanisms: a) heat conduction through the solid phase, b) heat conduction through the contact area, c) heat conduction through the fluid, and d) radiative heat transfer between the surfaces. Mechanisms b), c) and d) are thermally connected in parallel and these are thermally connected in series with mechanism a) which is negligibly small [16, 17].

The following assumptions are made: 1) the glass spheres are identical in size, 2) the spheres are smooth and clean, 3) the contact area is circular having a radius small relative to the sphere diameter, 4) elasticity theory can be used to predict the contact radius as a function of sphere diameter, load, elastic modulus and Poisson's ratio, 5) the simplest cubic packing model will be assumed, and 6) the typical element can be modelled as shown in Fig. 1, 7) radiation is neglected because the theory will be compared with test data obtained for microspheres at temperatures below 500 C, and 8) the total heat flow

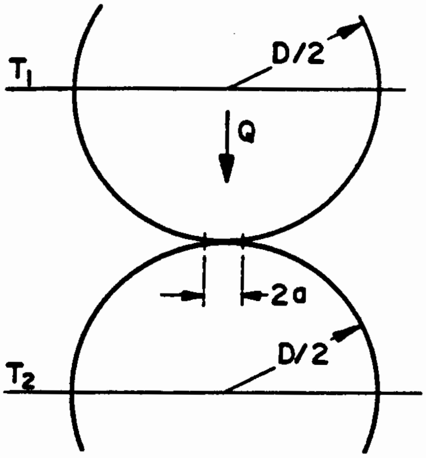

Fig. 1 Schematic of typical element

rate Q_T can be separated into two streams: Q_c crossing via the contact and Q_g crossing via the gas gap. For most porous substances Q_c is equal to or greater than Q_g, and the two streams can be separated within the solid phase as shown in Fig. 2.

Elastic Contact

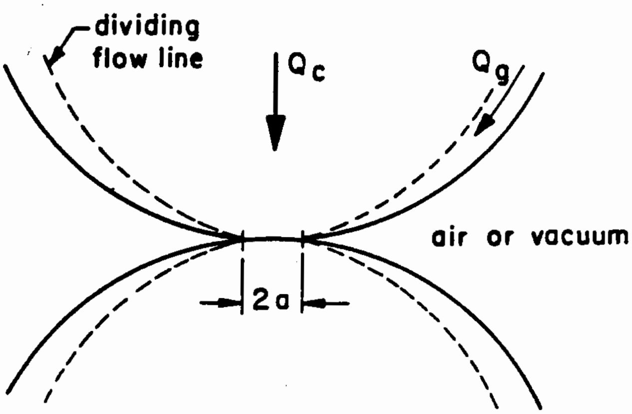

Fig. 2 Solid and gas heat flow streams

The elastic contact between identical spheres is given by [13]

$$\frac{2a}{D} = \frac{1}{L} = 1.44 \left[\frac{F(1-\nu^2)}{ED^2}\right]^{1/3} \tag{1}$$

where a is the contact radius, D is the sphere diameter, F is the contact force normal to the contact plane, ν is Poisson's ratio and E is the modulus of elasticity.

The air gap thickness δ at any point outside the contact can be evaluated by means of

$$L^2 \frac{\delta}{D} = \left\{\frac{2}{\pi} \sin^{-1} \frac{1}{x} - 1\right\} \left(1 - \frac{x^2}{2}\right) + \frac{1}{\pi} \sqrt{x^2 - 1} \tag{2}$$

which is based upon elasticity theory, or by means of a simpler geometric expression:

$$L \frac{\delta}{D} = \sqrt{L^2 - 1} - \sqrt{L^2 - x^2} \tag{3}$$

where x = r/a is the dimensionless radial position relative to the contact radius. The geometric expression will be used in this analysis because it is amenable to integration, and it has been shown [12] that there is little difference in the final result between the use of Eq. (2) or (3).

Constriction Resistance

If we assumed that $Q_c/Q_g > 1$, then the dividing flow line will be near the surface of the spherical particles and the resistance to heat flow within the solid phase is essentially the constriction resistance of a small circular contact area attached to a relatively large sphere. The total constriction resistance including both sides of a contact can be written as

$$R_c = \frac{\psi}{2ak_s} \tag{4}$$

where a is the contact radius, k_s is the solid conductivity and ψ is the thermal constriction factor.

The constriction factor is complex depending upon the geometry of the contact area, the geometry of the particle, and the boundary conditions. If the contact radius is very small relative to the diameter of the spherical particle, then the dependence of ψ upon the particle geometry becomes less important, and ψ is essentially a function of the boundary conditions alone. For constant temperature ψ = 1 and for constant heat flux ψ = 1.08. Whenever the relative size of the contact area becomes large ($2a/D \simeq 0.10$), or the ratio Q_c/Q_g approaches unity, then ψ = 1 or 1.08 will not be correct. As an approximation we will use [15]

$$\psi = 1 - \frac{4}{\pi} \left(\frac{2a}{D}\right) \tag{5}$$

as the constriction factor for 2a/D large and Q_c/Q_g near unity.

Equations (1), (3), (4) and (5) will be used in the decoupled and coupled models to follow.

<u>Decoupled Model</u>. This model will be based upon the following assumptions: 1) Q_c and Q_g are independent of each other, 2) the boundary of the gas region, except very near the contact, is essentially isothermal, 3) the heat flow lines within the gas region are all parallel being perpendicular to the contact plane, 4) the thermal conductivity of the gas is uniform, and 5) the thermal resistance of an elemental volume of the gas, Fig. 3a, is given by

$$dR_g = \frac{\delta}{k_g \, 2\pi r dr} \tag{6}$$

where k_g is the thermal conductivity of the gas under continuum conditions. The total conduction resistance, R_g, of the gas, after substitution of Eq. (3), is therefore

$$\frac{1}{R_g} = Dk_g \frac{\pi}{2L} \int_{\xi}^{L} \frac{x dx}{\sqrt{L^2 - 1} - \sqrt{L^2 - x^2}} \tag{7}$$

The lower limit of Eq. (7) cannot be unity because the integral is singular at this value of ξ, and also physically one cannot include the gas region adjacent

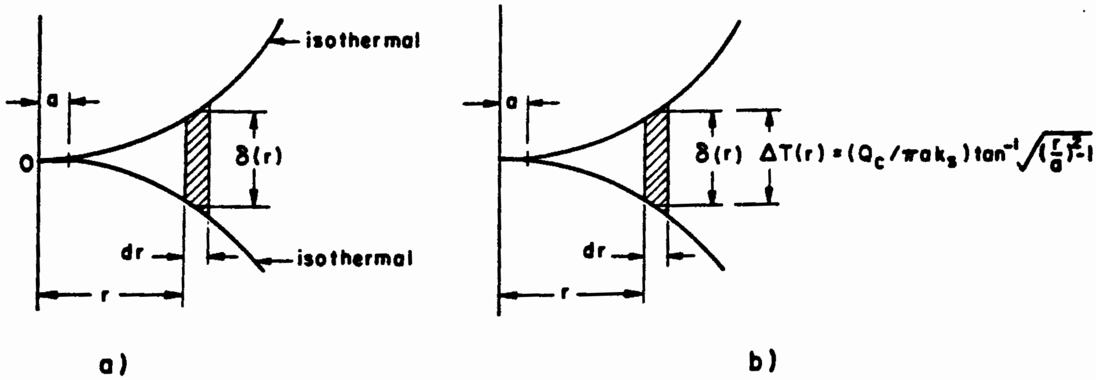

Fig. 3 Elemental volume for gas resistance
a) Decoupled b) Coupled

to the contact in evaluating Eq. (7) because here the Knudsen number approaches a very large value, indicating that the gas no longer behaves like a continuum. A lower limit different from unity must be used. Hence, for $\xi = \beta > 1$, Eq. (7) becomes

$$\frac{1}{D\,k_g\,R_g} = \frac{\pi}{2L}\left\{\sqrt{L^2-1}\,\ln\left(\frac{\sqrt{L^2-1}}{\sqrt{L^2-1}-\sqrt{L^2-\beta^2}}\right) - \sqrt{L^2-\beta^2}\right\} \tag{8}$$

The right-hand side of Eq. (8) will be defined as $\Phi_1(L,\beta)$ which is a dimensionless parameter depending upon the dimensionless contact and the lower limit β. It has been shown empirically [12, 13] that for L small, $\beta \doteq 2.2$ adequately correlates the resistance for two different sized sphere experiments.

The total resistance R_T of the typical element consists of the constriction and gas resistances thermally connected in parallel, therefore

$$\frac{1}{R_T} = \frac{1}{R_c} + \frac{1}{R_g} \tag{9}$$

neglecting any radiative effects. If we now consider the typical element of cross-section D^2, length D, and apparent conductivity k_a, its thermal resistance is given by

$$R_T = \frac{1}{Dk_a} \tag{10}$$

Equating Eqs. (9) and (10), solving for k_a, and dividing by the bulk thermal conductivity of the spheres yields the following dimensionless expression:

$$k_a^* = \frac{1}{Dk_s\,R_c} + \frac{1}{Dk_s\,R_g} \tag{11}$$

Upon substitution of Eqs. (4), (5) and (8) into Eq. (11) we get

$$k_a^* = \frac{1}{L\psi} + k_g^*\,\Phi_1 \tag{12}$$

where k_a^* is the dimensionless apparent conductivity and k_g^* is the dimensionless gas conductivity. Eq. (12) is valid provided the gas behaves like a continuum.

To model the effect of reduced gas pressures, an effective gas gap thickness is defined as that volume of gas having a heat flow area $(\pi D^2/4)(1 - 1/L^2)$, an effective thickness δ_e, and whose total resistance is equal to the gas resistance given by Eq. (8). This leads directly to an expression for the dimensionless effective gas thickness:

$$\delta_e^* = (\pi/4)/\Phi_1 \tag{13}$$

where $\delta_e^* = \delta_e/D$. It should be noted that δ_e^* is independent of the thermal conductivities of the solid and gas, but does depend upon the relative contact size. The effect of gas pressures below one atmosphere will be taken into account by utilizing an effective gas thermal conductivity at any pressure P_g and any temperature T which is related to the gas conductivity under atmospheric conditions in the following manner [14]:

$$\frac{k_g}{k_{g\infty}} = \left\{1 + 1.67\alpha\,\frac{\Lambda^*\,T^*}{\delta_e^*\,P_g^*}\right\}^{-1} \tag{14}$$

where α is the accomodation parameter given by $\alpha = (2 - \alpha_1)/\alpha_1 + (2 - \alpha_2)/\alpha_2$, $\Lambda^* = \Lambda/D$ is the dimensionless mean free path of the gas, $T^* = T/288$ is the dimensionless average absolute temperature of the gas, and $P_g^* = P_g/760$ is the dimensionless gas pressure. Eq. (14) is strictly valid for a diatomic gas layer bounded by parallel isothermal walls. It is assumed that Eq. (14) with Eq. (13) can be used to predict with reasonable accuracy the low gas pressure effects within the gas region shown in Fig. 3a.

For accomodation coefficients equal to unity, Eq. (12), with Eq. (14), becomes

$$k_a^* = \frac{1}{L\psi} + \frac{(\pi/4)\,k_{g\infty}^*}{\delta_e^* + 3.34\,\Lambda^* T^*/P_g^*} \tag{15}$$

Coupled Model. This model will be based upon the following assumptions: 1) Q_c is the primary heat flow and is independent of Q_g, 2) Q_g is the secondary heat flow and is dependent upon the temperature field set up by Q_c, 3) the temperature distribution over the boundary of the gas region can be determined by considering Q_c and the constriction resistance between the contact and some arbitrary point within the sphere, 4) the ratio Q_c/Q_g is at least equal to unity, but is normally greater than unity, so that Q_c flows through 70% or more of the cross-section of a sphere, 5) the thermal conductivity of the gas is uniform, and 6) the heat flow rate through an elemental volume of the gas, Fig. 3b, is given by the Fourier equation

$$dQ_g = \frac{k_g \, \Delta T(r) \, 2\pi r dr}{\delta} \tag{16}$$

Yovanovich [16, 17] has shown that the local temperature drop can be related to the heat flow rate through the contact, the contact radius and the thermal conductivity of the solid in the following manner:

$$\Delta T(r) = (Q_c/\pi a k_s) \tan^{-1} \sqrt{\left(\frac{r}{a}\right)^2 - 1} \tag{17}$$

In the coupled model it will be assumed that Eq. (17) is a good approximation of the local temperature drop across the elemental volume of gas.

Upon substitution of Eqs. (3) and (17) into Eq. (16) and integrating over the effective gas region, one gets the following dimensionless expression:

$$\left(\frac{Q_g}{Q_c}\right)\left(\frac{k_s}{k_g}\right) = \int_{\xi}^{L} \frac{x \tan^{-1}\sqrt{x^2 - 1} \, dx}{\sqrt{L^2 - 1} - \sqrt{L^2 - x^2}} \tag{18}$$

The lower limit in the integral cannot be unity. It has been shown [12, 13] that a lower limit of about 2.2 adequately describes the heat flow through the gas, and this value will be used in this analysis.

The total heat flow rate Q_T between adjacent spheres is the sum of the flows through the contact and the gas, therefore

$$Q_T = Q_c + Q_g = Q_c\{1 + k_g^* \, \Phi_2 \, (L,\beta)\} \tag{19}$$

where Φ_2 is the integral of Eq. (18).

The total resistance is by definition the effective total temperature drop divided by the total heat flow rate. The effective total temperature drop is assumed to be the temperature drop associated with Q_c and R_c without gas present. Therefore

$$R_T = \frac{\psi}{2k_s a[1 + k_g^* \, \Phi_2]} \tag{20}$$

The total resistance is also given by Eq. (10). Therefore equating Eqs. (10) and (20), solving for k_a and normalizing leads to

$$k_a^* = \{1 + k_g^* \, \Phi_2\}/L\psi \tag{21}$$

as the expression for the dimensionless apparent conductivity.

In order to utilize Eq. (21) at reduced gas pressures, an effective gas gap thickness is required. Persuing the logic presented under the decoupled model, it can be shown that for the coupled model the dimensionless effective gas gap thickness can be determined by means of

$$\delta_e^* = \frac{(\pi/4) \, L\psi}{\Phi_2} \tag{22}$$

Using Eq. (14) for the effective gas conductivity at reduced gas pressures, Eq. (21), upon substitution of $\alpha = 2$ for accomodation coefficients of unity, becomes

$$k_a^* = \{1 + \frac{k_{g\infty}^* \, \Phi_2}{1 + 3.34 \, \frac{\Lambda^* \, T^*}{\delta_e^* \, P_g^*}}\}/L\psi \tag{23}$$

DISCUSSION AND COMPARISON OF MODELS

Before comparing the results of the decoupled and coupled models with available test data the two models will be examined. It can be seen that both apparent conductivity expressions: Eq. (15), for the decoupled model, and Eq. (23), for the coupled model, yield the same value $k_a^* = 1/L\psi$ under vacuum conditions. If the contact force F were known, Eq. (1) would give L, Eq. (5) would be used to evaluate ψ and the reciprocal of the product of L and ψ would yield the contribution to the apparent conductivity due to the contacts. The effective dimensionless gas gap thickness δ_e^* can be determined by means of Eq. (13) and Eq. (22) for the decoupled and coupled models, respectively, after having determined Φ_1 and Φ_2. Finally, either Eq. (15), for the decoupled model, or Eq. (23), for the coupled model, can be used to determine the apparent conductivity at gas pressures from vacuum conditions to one atmosphere.

Since the contact force is not known for a particular system, the vacuum test conditions will be used to evaluate the parameter L. Both models under vacuum conditions lead to the same relationship between L and k_a^*, namely,

$$\frac{1}{L} = \frac{k_{av}^*}{1 + \frac{4}{\pi} k_{av}^*} \tag{24}$$

where k_{av}^* is the dimensionless apparent conductivity obtained from vacuum tests.

The validity of the two models will be compared with the test data of Dumez [8], and Masamune and Smith [11]. Dumez obtained apparent conductivity data for clean glass microspheres whose diameters ranged from 300 to 500 μ. The apparent density and porosity were reported to be 1.78 kg/litre and 33%, respectively. The tests were conducted in a cylindrical system filled with clean dry air whose pressure ranged from one atmosphere down to 0.01 mm Hg. Tests were conducted at several temperatures ranging from 273 K to 623 K. The theory presented in this paper will be compared with the 373 K and 473 K data. At these temperatures Dumez [8] reported the bulk conductivity to be 0.74 and 0.786 W/m K, respectively. The measured dimensionless apparent conductivity values are shown in Tables 5 and 6 below, for the Dumez [8] tests. For comparative purposes it will be assumed that the diameter of the microspheres [8] was 400 microns. Since Dumez reported bulk thermal conductivity values for the glass beads, these values were also used to normalize the second set of test data [11].

For convenience only, the two models, Eq. (15) and Eq. (23) have been rewritten in the following forms:

Decoupled Model

$$k_a^* = k_{av}^* + \frac{K_1}{\delta_e^* + \frac{K_2}{P_g}} \tag{25}$$

Coupled Model

$$k_a^* = k_{av}^* \left[1 + \frac{K_3}{1 + \frac{K_4}{\delta_e^* P_g}}\right] \tag{26}$$

where P_g is the gas pressure in mm Hg. The parameters K_1, K_2, K_3 and K_4 have been evaluated for air and glass beads at the test conditions reported [8, 11]. These parameters are presented for both sets of data in Tables 1, 2, 3 and 4. The effective dimensionless gas gap thickness is also presented in Tables 1, 2, 3 and 4 for both sets of data. Tables 1 and 2 correspond to the decoupled model, while Tables 3 and 4 correspond to the coupled model. It should be noted that both models yield similar values of δ_e^* for the two sets of data, namely $\delta_e^* = 0.130$ for the decoupled model and $\delta_e^* = 0.150$ for the coupled model. Tables 5 and 6 contain the data of Dumez [8], the predicted values of Eq. (25) and Eq. (26), as well as the ratios of the measured k_a^* to the predicted values of k_a^*. Tables 7, 8, 9 and 10 contain the variable sphere diameter data [11], the predicted values of Eq. (25) and Eq. (26), as well as the ratios of the measured k_a^* to the predicted values of k_a^*.

The agreement between the available test data [8, 11] and the two models, Eq. (25) and (26), can be seen in the last two columns. It is clear that the coupled model is superior to the decoupled model at gas pressures in excess of 5 mm Hg for both sets of data. The agreement between Eq. (26) which is based upon Eq. (23), the coupled model, and the Dumez data [8] is excellent at low gas pressures ($\leq$ 0.1 mm Hg) and reasonably good at high gas pressures ($\geq$ 300 mm Hg). The agreement between Eq. (26) and the other test data [11] is excellent for all sphere diameters at low gas pressures (< 0.5 mm Hg) and high gas pressures (> 500 mm Hg). The largest difference (about 10%) between theory and test data [11] occurs at different gas pressures depending upon the sphere diameter: 100 mm Hg for D = 29 μ, 50 mm Hg for D = 80 μ, 10 mm Hg for D = 200 μ and 5 mm Hg for D = 470 μ. The largest difference (about 21%) between Eq. (26) and test [8] occurs at a gas pressure of 6 mm Hg, consistent with that observed with the other test data [11].

Comparison with Kunii and Smith model [4]

This analysis based upon constriction resistance due to heat flowing through the contact area will be compared with the model of Kunii and Smith. In their model it was assumed that only point contact exists between spheres with all the heat crossing the contact plane by conduction through the gas only. They also assumed that there was no bending of heat flow lines within the solid and gas phases. They modelled their typical element as two cylindrical solids of flow area $\pi D^2/4$, and thickness 2D/3, separated by an effective gas gap thickness which can be calculated by means of the following expression:

$$\delta_e^* = \frac{0.50\,(1 - k_g^*)^2 \sin^2\theta_o}{\ln\{\frac{1}{k_g^*} - (\frac{1}{k_g^*} - 1)\cos\theta_o\} - (1 - k_g^*)(1 - \cos\theta_o)} - \frac{2}{3} k_g^* \tag{27}$$

where the parameter θ_o depends upon the packing; for close packing (ϕ = 0.260), θ_o = 22.3° and for loose packing (ϕ = 0.476), θ_o = 55.9°. For an intermediate packing (0.260 < ϕ < 0.476), they recommend a linear interpolation to determine the effective dimensionless gas gap thickness:

$$\delta_e^* = \delta_{e1}^* + (\delta_{e2}^* - \delta_{e1}^*)\left[\frac{\phi - 0.260}{0.216}\right] \tag{28}$$

Table 1 Parameters for decoupled model, Eq. (25), and Ref. [8].

T(°K)	373	473
k_{av}^*	0.0716	0.0730
δ_e^*	0.128	0.130
K_1	0.0331	0.0366
K_2	0.526	0.688

Table 2 Parameters for decoupled model, Eq. (25), and Ref. [11].

D(μ)	29	80	200	470
k_{av}^*	0.0714	0.0714	0.0714	0.0714
δ_e^*	0.130	0.130	0.130	0.130
K_1	0.0280	0.0280	0.0280	0.0280
K_2	6.31	2.29	0.915	0.390

Table 3 Parameters for coupled model, Eq. (26), and Ref. [8].

T(°K)	373	473
k_{av}^*	0.0716	0.0730
δ_e^*	0.150	0.152
K_3	3.08	3.31
K_4	0.542	0.688

Table 4 Parameters for coupled model, Eq. (26), and Ref. [11].

D(μ)	29	80	200	470
k_{av}^*	0.0714	0.0714	0.0714	0.0714
δ_e^*	0.151	0.151	0.151	0.151
K_3	2.60	2.60	2.60	2.60
K_4	6.31	2.29	0.915	0.390

P_g mm Hg	$k_a^*[8]$	k_a^*[Eq. (25)]	k_a^*[Eq. (26)]	$\frac{k_a^*[8]}{k_a^*\text{[Eq. (25)]}}$	$\frac{k_a^*[8]}{k_a^*\text{[Eq. (26)]}}$
760	0.295	0.319	0.291	0.924	1.010
300	0.278	0.317	0.290	0.876	0.960
30	0.227	0.291	0.268	0.779	0.847
6	0.162	0.222	0.209	0.731	0.775
0.6	0.0872	0.104	0.103	0.836	0.847
0.1	0.0750	0.0777	0.0775	0.968	0.968
0.01	0.0716	0.0722	0.0722	0.991	0.992

Table 5 Comparison of models and test data [8] at 373 K

P_g mm Hg	$k_a^*[8]$	k_a^*[Eq. (25)]	k_a^*[Eq. (26)]	$\frac{k_a^*[8]}{k_a^*\text{[Eq. (25)]}}$	$\frac{k_a^*[8]}{k_a^*\text{[Eq. (26)]}}$
760	0.340	0.355	0.313	0.958	1.086
300	0.330	0.352	0.311	0.937	1.061
30	0.266	0.314	0.283	0.847	0.940
6	0.168	0.223	0.211	0.752	0.796
0.6	0.0935	0.102	0.101	0.919	0.926
0.1	0.0780	0.0782	0.0782	0.997	0.997
0.01	0.0730	0.0735	0.0735	0.993	0.993

Table 6 Comparison of models and test data [8] at 473 K

P_g mm Hg	$k_a^*[11]$	k_a^*[Eq. (25)]	k_a^*[Eq. (26)]	$\frac{k_a^*[11]}{k_a^*\text{[Eq. (25)]}}$	$\frac{k_a^*[11]}{k_a^*\text{[Eq. (26)]}}$
760	0.248	0.271	0.247	0.915	1.004
500	0.236	0.265	0.243	0.890	0.971
100	0.188	0.215	0.202	0.873	0.931
50	0.162	0.181	0.172	0.895	0.942
10	0.1047	0.108	0.1072	0.969	0.977
5	0.0856	0.0915	0.0912	0.936	0.939
0.5	0.0714	0.0736	0.0736	0.970	0.970
0.1	0.0714	0.0718	0.0718	0.994	0.994
0.05	0.0714	0.0716	0.0718	0.997	1.000
0.01	0.0714	0.0714	0.0718	1.000	1.000

Table 7 Comparison of models and test data [11] at D = 29μ

P_g mm Hg	$k_a^*[11]$	k_a^*[Eq. (25)]	k_a^*[Eq. (26)]	$\frac{k_a^*[11]}{k_a^*\text{[Eq. (25)]}}$	$\frac{k_a^*[11]}{k_a^*\text{[Eq. (26)]}}$
760	0.255	0.279	0.253	0.914	1.008
500	0.249	0.276	0.252	0.903	0.988
100	0.216	0.252	0.233	0.862	0.927
50	0.193	0.231	0.214	0.835	0.902
10	0.133	0.149	0.145	0.893	0.917
5	0.112	0.119	0.117	0.941	0.957
0.5	0.0737	0.0773	0.0773	0.953	0.953
0.1	0.0714	0.0726	0.0726	0.983	0.983
0.05	0.0714	0.0720	0.0714	0.992	1.000
0.01	0.0714	0.0714	0.0714	1.000	1.000

Table 8 Comparison of models and test data [11] at D = 80μ

P_g mm Hg	$k_a^*[11]$	k_a^*[Eq. (25)]	k_a^*[Eq. (26)]	$\frac{k_a^*[11]}{k_a^*\text{[Eq. (25)]}}$	$\frac{k_a^*[11]}{k_a^*\text{[Eq. (26)]}}$
760	0.257	0.282	0.256	0.912	1.004
500	0.225	0.281	0.255	0.907	1.000
100	0.236	0.270	0.246	0.873	0.959
50	0.219	0.260	0.237	0.842	0.924
10	0.166	0.197	0.187	0.843	0.888
5	0.140	0.161	0.155	0.870	0.903
0.5	0.0904	0.0857	0.0855	1.055	1.057
0.1	0.0785	0.0744	0.0744	1.055	1.055
0.05	0.0737	0.0729	0.0729	1.011	1.011
0.01	0.0714	0.0717	0.0717	0.996	0.996

Table 9 Comparison of models and test data [11] at D = 200μ

P_g mm Hg	$k_a^*[11]$	k_a^*[Eq. (25)]	k_a^*[Eq. (26)]	$\frac{k_a^*[11]}{k_a^*[\text{Eq. (25)}]}$	$\frac{k_a^*[11]}{k_a^*[\text{Eq. (26)}]}$
760	0.257	0.283	0.256	0.908	1.003
500	0.257	0.282	0.256	0.911	1.004
100	0.252	0.277	0.252	0.910	1.000
50	0.240	0.275	0.248	0.873	0.968
10	0.197	0.235	0.219	0.838	0.900
5	0.174	0.206	0.194	0.845	0.897
0.5	0.107	0.102	0.102	1.049	1.049
0.1	0.0856	0.0784	0.0783	1.092	1.093
0.05	0.0808	0.0749	0.0749	1.079	1.079
0.01	0.0737	0.0721	0.0721	1.022	1.022

Table 10 Comparison of models and test data [11] at D = 470μ.

Otherwise they recommend that one put

$$\delta_e^* = \delta_{e1}^* \quad \text{for} \quad \phi \le 0.260$$

and (29)

$$\delta_e^* = \delta_{e2}^* \quad \text{for} \quad \phi \ge 0.476$$

where δ_{e1}^* corresponds to close packed beds and δ_{e2}^* corresponds to loose packed beds.

For negligible radiation effects their model leads to the following expression for the dimensionless apparent conductivity:

$$k_a^*/k_g^* = \phi + (1 - \phi)/(\delta_e^* + \frac{2}{3} k_g^*) \qquad (30)$$

It will be noted that the Kunii-Smith model depends upon the solid/gas conductivities and the packing arrangement, but is independent of sphere size and any loading parameter. This model cannot be used to predict low gas pressure effects nor apparent conductivities under vacuum conditions.

The comparison between test data [8, 11] and the Kunii-Smith model [4] is summarized in Table 11. The comparison can only be made at atmospheric conditions because Kunii and Smith did not take into account the effect of contact areas. It can be seen in Table 11 that there is good agreement between theory and test [8] at 373 K and moderate agreement at 573 K when the porosity is 0.33. The 20% difference between theory and test data [11] is also observed when the porosity is 0.38 and the temperature is 315 K for all sphere diameters.

The coupled model proposed in this study based upon the simple cubic packing is superior to the Kunii and Smith model for the glass bead/air system at atmospheric pressure, and for reduced air pressures as well.

CONCLUDING REMARKS

A method has been proposed to predict the apparent conductivity of glass microspheres in terms of the system physical and thermal properties, the system geometry as well as the system temperature and pressure. It has been demonstrated that both the decoupled and coupled models agree quite well with available test data at low and high air pressures, and reasonably well at moderate gas pressures. It was shown that test data under vacuum conditions

Table 11 Comparison of Kunii-Smith model [4] with test data [8, 11]

$T(^oK)$	373 [8]	573 [8]	315 [11]
ϕ	0.33	0.33	0.38
δ_e^*	0.0742	0.0775	0.0911
k_a^*	0.283	0.322	0.213
$k_a^*[8]$	0.295	0.391	—
$k_a^*[11]$	—	—	0.255
$\frac{k_a^*(\text{test})}{k_a^*(\text{k-s})}$	1.042	1.214	1.197

can be used to determine the effective loading between the contacting spheres, as well as the contribution of the contact areas to the apparent conductivity of the system over the entire pressure range. For the glass beads/air system the model proposed here is superior to the Kunii-Smith model.

ACKNOWLEDGEMENTS

The author acknowledges the financial assistance of the National Research Council of Canada. W.W. Kitscha's efforts are also acknowledged.

REFERENCES

1 Fulk, M.M., "Evacuated Powder Insulation for Low Temperatures", Progress in Cryogenics, Vol. 1, 1959, pp. 65-84.

2 Argo, W.B. and Smith, J.M., "Heat Transfer in Packed Beds", Chem. Eng. Progress, Vol. 49, No. 8, pp. 443-451.

3 Yagi, S. and Kunii, D., "Studies on Effective Thermal Conductivities in Packed Beds", A.I.Ch.E. Journal, pp. 373-381, Vol. 3, No. 3, Sept. 1957.

4 Kunii, D. and Smith, J.M., "Heat Transfer Characteristics of Porous Rocks", A.I.Ch.E. Journal, pp. 71-78, Vol. 6, No. 1, March 1960.

5 Woodside, W. and Messmer, J.H., "Thermal Conductivity of Porous Media. I. Unconsolidated Sands; II. Consolidated Rocks", Journal of Applied Physics, Vol. 32, No. 9, pp. 1688-1706, Sept. 1961.

6 Chen, J.C. and Churchill, S.W., "Radiant Heat Transfer in Packed Beds", A.I.Ch.E. Journal, pp. 35-41, Vol. 9, No. 1, January 1963.

7 Dumez, P., "La Conductivité Thermique des Matériaux Pulvérulents et Granulaires et ses Méthodes de Mesure en Régime Etabli", Part 1, Révue Générale de Thermique, No. 54, pp. 561-574, Juin, 1966.

8 Dumez, P., "La Conductivité Thermique des Matériaux Pulvérulents et Granulaires et ses Méthodes de Mesure en Régime Etabli", Part 11, Révue Générale de Thermique, No. 55, pp. 673-686, Juillet, 1966.

9 Luikov, A.V., Shaskov, A.G., Vasiliev, L.L. and Fraiman, Yu, E., "Thermal Conductivity of Porous Systems", Int. J. Heat Mass Transfer, Vol. 11, pp. 117-140, 1968.

10 Wakao, N., Kato, K. and Furuya, N., "View Factor Between Two Hemispheres in Contact and Radiation Heat-Transfer Coefficient in Packed Beds", Int. J. Heat and Mass Transfer, Vol. 12, pp. 118-120, 1969.

11 Masamune, S. and Smith, J.M., "Thermal Conductivity of Spherical Particles", Ind. Eng. Chem. Fundamentals, Vol. 2, pp. 136-143, 1963.

12 Kitscha, W.W., M.A.Sc. Thesis, Dept. of Mech. Eng. University of Waterloo, in progress.

13 Yovanovich, M.M. and Kitscha, W.W., "Modeling the Effect of Air and Oil Upon the Thermal Resistance of a Sphere-Flat Contact", AIAA Paper, To be presented at the AIAA 8th Thermophysics Conference, Palm Springs, Calif., July 16-18, 1973.

14 Kennard, E.H., Kinetic Theory of Gases, McGraw-Hill Book Co. Inc., New York, 1938.

15 Yovanovich, M.M., "Sur la Conductivité Thermique Apparente D'un Ensemble de Billes Sous Vide", Submitted to Can. Soc. Mech. Eng.

16 Yovanovich, M.M., Cordier, H. and Coutanceau, J., "Sur la résistance thermique due à un contact unique de section circulaire", C.R. Acad. Sc. Paris, t. 268, pp. 1-4, January 1969.

17 Yovanovich, M.M., "A General Expression for Predicting Conduction Shape Factors", AIAA Paper No. 73-121, AIAA 11th Aerospace Sciences Meeting, Washington, D.C., January 10-12, 1973.